Effect of temperature on quantum criticality in the frustrated two-leg Heisenberg ladder

Brandon W. Ramakko and Mohamed Azzouz*
Department of Physics, Laurentian University, Ramsey Lake Road, Sudbury, Ontario, Canada, P3E 2C6
(Received 16 February 2007; revised manuscript received 30 April 2007; published 16 August 2007)

The antiferromagnetic Heisenberg model on the two-leg ladder with exchange interactions along the chains, rungs, and diagonals is studied using the Jordan-Wigner transformation and bond-mean-field theory. The inclusion of all three couplings introduces frustration to the system and depending on their relative strengths the ladder can adopt one of three possible magnetically disordered gapped states. The phase diagram found in this mean-field approach is in very good agreement with the one calculated by Weihong *et al.* [Phys. Rev. B **57**, 11439 (1998)] using the Lanczos exact diagonalization method. By analyzing the ground-state energy, we study quantum criticality when the coupling parameters are varied at zero temperature. We study the effect of temperature on the phase boundaries and find that the system shows thermally induced criticality for some values of the rung and diagonal coupling constants. All the phase transitions encountered in this system occur between disordered phases and are all caused by frustration.

DOI: 10.1103/PhysRevB.76.064419 PACS number(s): 75.10.Jm, 75.40.−s, 73.43.Nq

I. INTRODUCTION

Quantum criticality is a current highly debated issue in strongly correlated electron systems.[1] There are three kinds of strongly correlated systems. The first ones are those with only localized electrons like the quantum Heisenberg-type spin systems, where only the spin degrees of freedom contribute to the physical properties. The second ones are those systems where electrons are mobile, and both the spin and electron degrees of freedom are relevant like in the high-T_C materials away from half-filling. The third type of systems are those fermionic systems with both localized and itinerant electrons like in the Kondo-type (heavy-fermion) systems. In this work, we develop an analytical approach to study the quantum criticality phenomenon in the frustrated antiferromagnetic (AF) two-leg Heisenberg ladder and the effect of temperature on this criticality. Because absolute zero temperature cannot be reached in any experiment, it is important to investigate such temperature dependence. In the absence of frustration, the two-leg ladder has been analyzed extensively both numerically and analytically.[2] The case with second-nearest-neighbor interactions along the diagonals is of interest because this interaction adds frustration to the system, and there is a possibility that in real two-leg ladder materials it might be significant. Some examples of real two-leg ladder materials are $SrCu_2O_3$,[3] $Cu_2(C_5H_{12}N_2)_2Cl_4$,[4,5] and $La_6Ca_8Cu_{24}O_{41}$.[6,7] Existing numerical data on the frustrated ladder indicate that when the diagonal interaction is varied, the system undergoes a quantum phase transition. The main motivation for the present work is to reach better understanding of quantum criticality in the frustrated two-leg ladder from a microscopic point of view and to study the effect of temperature on it. the method we develop is an analytical approach based on the Jordan-Wigner (JW) transformation. It is first tested at zero temperature by making sure that it reproduces all the numerically derived exact existing results, then it is applied at finite temperature.

The Hamiltonian for the spin-$\frac{1}{2}$ two-leg ladder with diagonal interactions is written as

$$H = J\sum_{i}^{N}\sum_{j=1}^{2}\mathbf{S}_{i,j}\cdot\mathbf{S}_{i+1,j} + J_{\perp}\sum_{i}^{N}\mathbf{S}_{i,1}\cdot\mathbf{S}_{i,2} + J_{\times}\sum_{i}^{N}(\mathbf{S}_{i,1}\cdot\mathbf{S}_{i+1,2} + \mathbf{S}_{i+1,1}\cdot\mathbf{S}_{i,2}), \quad (1)$$

where J is the coupling along the chains, $J_{\perp}$ the transverse coupling, and $J_{\times}$ the coupling along the diagonals, as seen in Fig. 1. The index i labels the position of the spins along the two chains, each of which has N sites. The first term sums the interactions of nearest-neighboring spins along the chains (legs) of the ladder, the second term sums the interactions of the spins along the rungs, and the third term sums the interactions along the diagonals. As usual, $\mathbf{S}_{i,j}$ is the spin operator.

The frustrated two-leg ladder has been studied numerically using Ising and dimer expansions,[8] Lanczos diagonalization technique,[7–10] and the density-matrix renormalization group (DMRG).[10–14] It has also been studied analytically and we will next summarize briefly the different analytical theories that have been applied at zero temperature. The (dimerized) valence-bond spin-wave theory by Xian[15] was used to study the system. This theory breaks down for certain values of the couplings. For example, it works for $J/J_{\perp}<1/2$ (so in the strong coupling limit with $J_{\perp}\gg J$) when $J_{\times}/J_{\perp}=0$. The Abelian bosonization technique applied by Weighong *et al.*[8] and the non-Abelian bosonization method applied by Allen *et al.*[16] work only in the weak coupling limit $J_{\times},J_{\perp}<J$. The Lieb-Mattis theorem applied by Hakobyan[17] puts limits on the transition line such as $J_{\perp}\leqslant 2J_{\times}$ but cannot determine its exact position. The reformulated weak coupling field theory of Starykh and Balents[18] works in the limit $J_{\times},J_{\perp}<J$ only.

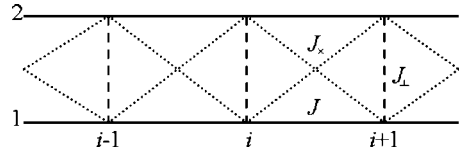

FIG. 1. The two-leg ladder showing the couplings along the chains, rungs, and diagonals is displayed.

These authors found that in the quantum model, the classical transition at $J_\perp = 2J_\times$ splits into two, implying the occurrence of a new phase, which was later disproved numerically.[10] The nonlinear sigma model was considered by Nedelcu *et al.*,[19] who focused on the case where the diagonal couplings are different. However, for the case with equal diagonal interactions, there are portions of the phase diagram where their theory fails. The nonperturbative effective field theory of Cabra *et al.*[20] examined which spin bonds are the strongest in order to put limits on weak and strong coupling regimes. However, no zero-temperature phase diagram was produced in their work.

None of these analytical methods was able to create a complete phase diagram including the weak, intermediate, and strong coupling regimes, which compares well with numerical data because of their various limitations. The exact numerical methods provide reliable information about the states of the system but in order to understand even these numerical results, one needs to develop analytical approaches, which are readily generalizable to finite temperature and which apply to all coupling regimes. Using the bond-mean-field theory[21–24] (BMFT), we seek better understanding of the phases of the frustrated two-leg ladder at both zero and nonzero temperatures. The BMFT is a mean-field theory that is based on the spin bond parameters. These parameters are not related in any way to any kind of long-range order. They are rather related to the spin-spin correlation function $\langle S_i^- S_j^+ \rangle$, with i and j labeling adjacent sites in the direction where this correlation function is calculated. All quantities $\langle S_i^\alpha \rangle$, with $\alpha = x, y, z$, are zero in BMFT, implying the absence of any sort of long-range magnetic order.

This paper is organized as follows. In Sec. II, we explain how the BMFT, which is based on the two-dimensional JW transformation, is applied to the Hamiltonian for the two-leg ladder with interactions along the chains, rungs, and diagonals. The Hamiltonian is handled and decoupled similarly to that of Ref. 21. Quantum criticality, energy spectra, mean-field parameters, free energy, entropy, and specific heat are calculated in Sec. III. Also, the zero and nonzero-temperature phase diagrams are calculated. Criticality at nonzero temperature is examined in Sec. IV. Discussion of our results is made in Sec. V. In Sec. VI, conclusions are drawn.

II. METHOD

In the Ising limit, where quantum spin fluctuations are absent, the magnetically ordered ground states are shown in the left panel of Fig. 2. Depending on the relative strength of the couplings, the system can be found in one of the three different ordered states displayed on the left of this figure. When $J_\times \ll J_\perp$, the system adopts the Néel state with ferromagnetic spin arrangements along the diagonals. When $J_\times \gg J_\perp$, the system adopts the ferromagnetic rung state. In this case, the AF arrangement shifts to the diagonals, and spins on the rungs are forced to adopt a ferromagnetic arrangement. When $J_\times \gg J$ and $J_\perp \gg J$, the system adopts a ferromagnetic chain state, where the spins on the chains are ordered ferromagnetically and antiferromagnetically on the rungs. The phase diagram in this classical limit will also be given later on for comparison.

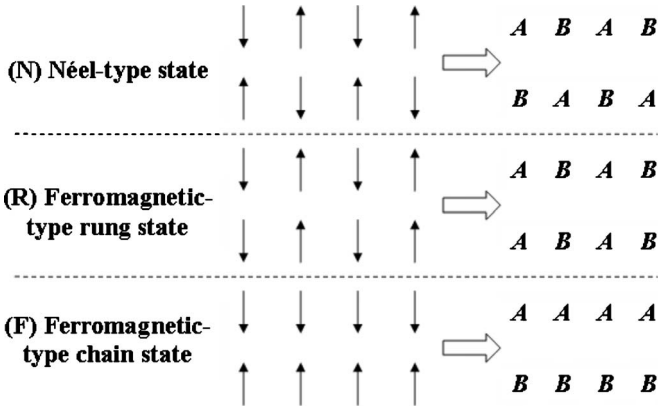

FIG. 2. In the left panel, the three possible ground states of the system in the Ising limit, namely, the Néel state, the ferromagnetic chain state, and the ferromagnetic rung state, are drawn. In the right panel, the labeling of sublattices corresponding to the short-range spin orders that replace the long-range ones is shown for the Heisenberg limit.

In the Heisenberg limit with full quantum fluctuations, we assume that in a one-to-one correspondence each of the magnetic orders in Fig. 2 evolves into a state which is characterized by only short-range order of the same kind as in the ordered state. So, we replace the rigid up and down orientations of the spins by sublattice labels A and B, respectively, as shown in the right panel of Fig. 2. According to Ref. 11, the boundaries in the phase diagram of the Ising limit move as a consequence of quantum fluctuations, but the number of phases stays the same, namely, 3. For this reason, we continue to label the phases using the same terms as in the Ising limit except that we now add the word type to indicate that the phases are not magnetically ordered but are rather characterized by short-range order only. So, the phases are now called the Néel-type (N-type) state, the ferromagnetic-type rung (R-type) state, and the ferromagnetic-type chain (F-type) state. For the N-type state in the absence of frustration, the ground state of the two-leg ladder is a gapped disordered spin liquid dominated by short-range AF correlations for any nonzero $J_\perp$.[2] The gap increases linearly with rung coupling, except near zero coupling where a slight downward curvature is present. The ferromagnetic-type rung state is also referred to as the Haldane phase or rung triplet phase because in this case the system presents some resemblance to the $S=1$ chain. Precisely, in the case $J_\perp = 0$ and $J_\times = J$, the Hamiltonian becomes $H = J\Sigma_i(\mathbf{S}_{i,1} + \mathbf{S}_{i,2}) \cdot (\mathbf{S}_{i+1,1} + \mathbf{S}_{i+1,2})$, with low-lying excitations identical to those of the $S=1$ Haldane chain due to the fact that the interaction is now between the resultant of the two spins on the rungs.[11] The N- and F-type states are also known as the dimerized or singlet states because of the formation of singlets along the rungs in the quantum case. The two phases belong to the same universality class so they are only topologically distinct due to the symmetry of the system.[12,25] For the N-type state, in the limit $J_\perp = \infty$ and $J_\times = 0$, the ground state is made of independent rung singlets.

We use the spin arrangements on the right panel in Fig. 2 as a starting point. We assume that in the Heisenberg limit,

short-range AF correlations are important enough to justify its use. Note that these spin arrangements are not static in the quantum limit but fluctuate while the relative average orientations of adjacent spins remain the same. We will confirm that the frustrated two-leg ladder is characterized by quantum criticality (criticality at zero temperature induced solely by quantum fluctuations) and show that it is also characterized by criticality at nonzero temperature. The finite-temperature phase transitions we propose for this practically one-dimensional system are not from order to disorder but they are from a disordered phase to another disordered one, i.e., between states that differ by their short-range magnetic order only.

A. Jordan-Wigner transformation and bond-mean-field theory

The JW transformation for the two-leg Heisenberg ladder is defined as[21]

$$S^{-}_{i,j} = c_{i,j} e^{i\phi_{i,j}},$$

$$S^{z}_{i,j} = n_{i,j} - 1/2, \quad n_{i,j} = c^{\dagger}_{i,j} c_{i,j},$$

$$\phi_{i,1} = \pi \left[\sum_{d=0}^{i-1} \sum_{f=1}^{2} n_{d,f} \right] \quad \text{for chain 1},$$

$$\phi_{i,2} = \pi \left[\sum_{d=0}^{i-1} \sum_{f=1}^{2} n_{d,f} + n_{i,1} \right] \quad \text{for chain 2}. \tag{2}$$

Here, i and j are the coordinates along the chain and rung directions, respectively. The phases $\phi_{i,j}$ are chosen so that all the spin commutation relations are preserved. The $c^{\dagger}_{i,j}$ operator creates a spinless fermion at site (i,j), while $c_{i,j}$ annihilates one, and $n_{i,j}$ is the occupation number operator.

After applying the JW transformation [Eq. (2)] to the Hamiltonian [Eq. (1)], we get

$$\begin{aligned} H = H_{XY} &+ J \sum_{i}^{N} \sum_{j=1}^{2} \left(c^{\dagger}_{i,j} c_{i,j} - \frac{1}{2} \right) \left(c^{\dagger}_{i+1,j} c_{i+1,j} - \frac{1}{2} \right) \\ &+ J_{\perp} \sum_{i}^{N} \left(c^{\dagger}_{i,1} c_{i,1} - \frac{1}{2} \right) \left(c^{\dagger}_{i,2} c_{i,2} - \frac{1}{2} \right) \\ &+ J_{\times} \sum_{i}^{N} \left[\left(c^{\dagger}_{i,1} c_{i,1} - \frac{1}{2} \right) \left(c^{\dagger}_{i+1,2} c_{i+1,2} - \frac{1}{2} \right) \right. \\ &\left. + \left(c^{\dagger}_{i+1,1} c_{i+1,1} - \frac{1}{2} \right) \left(c^{\dagger}_{i,2} c_{i,2} - \frac{1}{2} \right) \right], \end{aligned} \tag{3}$$

where

$$\begin{aligned} H_{XY} = &\frac{J}{2} \sum_{i}^{N} \left[c^{\dagger}_{i,1} e^{i\pi n_{i,2}} c_{i+1,1} + c^{\dagger}_{i,2} e^{i\pi n_{i+1,1}} c_{i+1,2} + \text{H.c.} \right] \\ &+ \frac{J_{\perp}}{2} \sum_{i}^{N} \left[c^{\dagger}_{i,1} c_{i,2} + \text{H.c.} \right] \\ &+ \frac{J_{\times}}{2} \sum_{i}^{N} \left[c^{\dagger}_{i,1} e^{i\pi (n_{i,2} + n_{i+1,1})} c_{i+1,2} + c^{\dagger}_{i+1,1} c_{i,2} + \text{H.c.} \right] \end{aligned} \tag{4}$$

is the XY Hamiltonian of the frustrated two-leg ladder. In BMFT, the interacting terms of the JW fermions are decoupled using the spin bond parameters. This approximation neglects fluctuations around the mean-field points: $(O - \langle O \rangle) \times (O' - \langle O' \rangle) \approx 0$, where O and O' are any operators which are quadratic in $c^{\dagger}$ and c.[22] This yields

$$OO' \approx \langle O \rangle O' + O \langle O' \rangle - \langle O \rangle \langle O' \rangle. \tag{5}$$

To apply BMFT, we introduce three mean-field bond parameters: Q in the longitudinal direction, P in the transverse direction, and P' along the diagonal. These can be interpreted as effective hopping energies for the JW fermions[23] in the longitudinal, transverse, and diagonal directions, respectively,

$$Q = \langle c_{i,j} c^{\dagger}_{i+1,j} \rangle,$$

$$P = \langle c_{i,j} c^{\dagger}_{i,j+1} \rangle,$$

$$P' = \langle c_{i+1,j} c^{\dagger}_{i,j+1} \rangle. \tag{6}$$

Keeping in mind that there is no long-range order[26] so that $\langle S^{z}_{i,j} \rangle = \langle c^{\dagger}_{i,1} c_{i,1} \rangle - 1/2 = 0$, the Ising quartic terms in Eq. (3) can be decoupled and simplified using the Hartree-Fock approximation [Eq. (5)] and the bond parameters [Eq. (6)] as follows:

$$\begin{aligned} \left(c^{\dagger}_{i,1} c_{i,1} - \frac{1}{2} \right) \left(c^{\dagger}_{i+1,1} c_{i+1,1} - \frac{1}{2} \right) &\approx c^{\dagger}_{i,1} c_{i+1,1} \langle c_{i,1} c^{\dagger}_{i+1,1} \rangle \\ &+ \langle c^{\dagger}_{i,1} c_{i+1,1} \rangle c_{i,1} c^{\dagger}_{i+1,1} \\ &- \langle c^{\dagger}_{i,1} c_{i+1,1} \rangle \langle c_{i,1} c^{\dagger}_{i+1,1} \rangle \\ &= Q c^{\dagger}_{i,1} c_{i+1,1} + Q^{*} c^{\dagger}_{i+1,1} c_{i,1} \\ &+ |Q|^2. \end{aligned} \tag{7}$$

Note that when decoupled in the magnetization channel, the quartic terms give $\left(c^{\dagger}_{i,1} c_{i,1} - \frac{1}{2} \right) \left(c^{\dagger}_{i+1,1} c_{i+1,1} - \frac{1}{2} \right) \approx 0$, which is a consequence of the absence of magnetic long-range order. Then, the Hamiltonian becomes

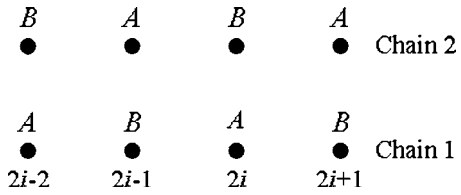

FIG. 3. The lattice is subdivided into two sublattices in the case of the N-type state.

$$
\begin{aligned}
H = H_{XY} + J\sum_{i}^{N}\sum_{j=1}^{2}[Qc_{i,j}^{\dagger}c_{i+1,j} + Q^{*}c_{i+1,j}^{\dagger}c_{i,j}] \\
+ J_{\perp}\sum_{i}^{N}[Pc_{i,1}^{\dagger}c_{i,2} + P^{*}c_{i,2}^{\dagger}c_{i,1}] \\
+ J_{\times}\sum_{i}^{N}[P'c_{i,1}^{\dagger}c_{i+1,2} + P'^{*}c_{i+1,2}^{\dagger}c_{i,1} + P'c_{i+1,1}^{\dagger}c_{i,2} \\
+ P'^{*}c_{i,2}^{\dagger}c_{i+1,1}] \\
+ 2NJ_{\times}|P'|^{2} + 2NJ|Q|^{2} + NJ_{\perp}|P|^{2}. \qquad (8)
\end{aligned}
$$

Next, we write this Hamiltonian using the three different spin configurations in the right panel of Fig. 2. These configurations are instantaneous (not static) configurations in which adjacent spins in any direction keep on average the same relative orientations with respect to each other but fluctuate globally on a time scale determined by the strongest coupling constant so that any kind of long-range magnetic order is absent. These fluctuations are a consequence of the quantum fluctuations. The three competing configurations of Fig. 2 lead to three different quantum gapped spin liquid states, each characterized by its own short-range spin correlations and symmetry.

B. Néel-type state

In the N-type state, the spin arrangement at any time consists on average of antiparallel spins on adjacent sites in both the longitudinal and rung directions; the spins on the diagonals thus prefer to align parallel to each other. In the limit $J_{\times} \ll J, J_{\perp}$, spins tend to form loose spin singlets on adjacent sites along both the chains and rungs if $J_{\perp} \sim J$ but strong spin singlets on the rungs if $J_{\perp} \gg J \gg J_{\times}$. The word Néel is not used to indicate long-range order but only the fact that the spin orientations show short AF order. For this reason, we divide the lattice into two sublattices; there are $c_{i,j}^{A}$ fermions on sublattice A and $c_{i',j'}^{B}$ on sublattice B, where (i',j') is any adjacent site to (i,j), Fig. 3.

Following Ref. 27, we set the average phase per plaquette to be π. We choose the configuration seen in Fig. 4 which was suggested by Azzouz *et al.* in Ref. 21. In the latter, this configuration is used to get rid of the phase terms in the XY Hamiltonian H_{XY}; the only effect is that the sign of the hopping term in the JW XY term becomes alternated along the chains. For the Ising term, we set $Q_{i,j}=Qe^{i\phi_{i,j}}$, where Q is site independent.[24] Here, $\phi_{i,j}$ is the phase of the bond corresponding to Fig. 4 such that $\phi=\pi$ or 0 along the chains,

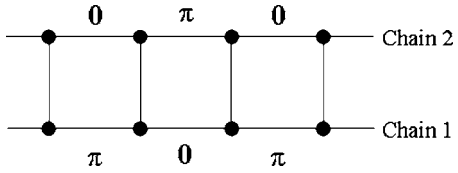

FIG. 4. The phase π alternates along the chains and is zero everywhere else. The flux per plaquette is π on average (Ref. 27).

which means that the Q terms alternate sign along the chains just like the XY terms do. This is necessary in order to recover the proper result in the limit $J_{\times}$ and $J_{\perp}$ go to 0, in which we get a result comparable to that of des Cloiseaux and Pearson[28] for the spin excitation spectrum for a single Heisenberg chain, namely, $E(k)=\frac{\pi}{2}J|\sin k|$. The alternating sign for Q can be justified in the same way as in Ref. 24.

A one-dimensional (1D) Fourier transform along the chains is performed on the Hamiltonian, keeping the chain index in the real space. The mean-field Hamiltonian can be expressed in the form

$$H = \sum_{k} \Psi_{k}^{\dagger}\mathcal{H}\Psi_{k} + 2NJQ^{2} + NJ_{\perp}P^{2} + 2NJ_{\times}P'^{2}, \qquad (9)$$

with the Nambu spinor defined by

$$\Psi^{\dagger} = (c_{1k}^{A\dagger}\ c_{1k}^{B\dagger}\ c_{2k}^{A\dagger}\ c_{2k}^{B\dagger}), \qquad (10)$$

and the Hamiltonian density given by

$$
\mathcal{H} = \begin{pmatrix}
0 & iJ_1\sin k & J_{\times 1}\cos k & \frac{J_{\perp 1}}{2} \\
-iJ_1\sin k & 0 & \frac{J_{\perp 1}}{2} & J_{\times 1}\cos k \\
J_{\times 1}\cos k & \frac{J_{\perp 1}}{2} & 0 & iJ_1\sin k \\
\frac{J_{\perp 1}}{2} & J_{\times 1}\cos k & -iJ_1\sin k & 0
\end{pmatrix}, \qquad (11)
$$

with

$$
\begin{aligned}
J_1 &= J(1+2Q), \\
J_{\perp 1} &= J_{\perp}(1+2P), \\
J_{\times 1} &= J_{\times}(1+2P'). \qquad (12)
\end{aligned}
$$

Diagonalizing $\mathcal{H}$ yields the energy eigenvalues $\pm E_{N1}$ and $\pm E_{N2}$, where

$$
\begin{aligned}
E_{N1}(k) &= J_{\times 1}\cos k + \sqrt{J_1^2\sin^2 k + \frac{J_{\perp 1}^2}{4}}, \\
E_{N2}(k) &= J_{\times 1}\cos k - \sqrt{J_1^2\sin^2 k + \frac{J_{\perp 1}^2}{4}}. \qquad (13)
\end{aligned}
$$

Note that the subscript N in E_{Np} is used to remind ourselves of the N-type state. Similarly, the eigenenergies of each of

the remaining states will be labeled using its appropriate subscript. The free energy corresponding to our Hamiltonian is

$$F = JQ^2 + \frac{J_\perp P^2}{2} + J_\times P'^2 - \frac{k_B T}{4N} \sum_k \sum_{s=\pm} \sum_{p=1,2} \ln[1 + e^{s\beta E_{Np}(k)}]. \tag{14}$$

The parameters are determined by minimizing F with respect to Q, P, and P', a calculation which leads to the following set of self-consistent equations:

$$Q = \frac{1}{8NJ} \sum_k \sum_{p=1,2} \frac{\partial E_{Np}(k)}{\partial Q} \tanh\left[\frac{\beta E_{Np}(k)}{2}\right],$$

$$P = \frac{1}{4NJ_\perp} \sum_k \sum_{p=1,2} \frac{\partial E_{Np}(k)}{\partial P} \tanh\left[\frac{\beta E_{Np}(k)}{2}\right],$$

$$P' = \frac{1}{8NJ_\times} \sum_k \sum_{p=1,2} \frac{\partial E_{Np}(k)}{\partial P'} \tanh\left[\frac{\beta E_{Np}(k)}{2}\right]. \tag{15}$$

The partial derivatives of the energies with respect to Q, P, and P' are given by

$$\frac{\partial E_{Np}}{\partial Q} = \frac{(-1)^{p+1} 2JJ_1 \sin^2 k}{\sqrt{J_1^2 \sin^2 k + \left(\frac{J_{\perp 1}}{2}\right)^2}},$$

$$\frac{\partial E_{Np}}{\partial P} = \frac{(-1)^{p+1} J_\perp J_{\perp 1}}{2\sqrt{J_1^2 \sin^2 k + \left(\frac{J_{\perp 1}}{2}\right)^2}},$$

$$\frac{\partial E_{Np}}{\partial P'} = 2J_\times \cos k \quad \text{with } p = 1,2. \tag{16}$$

Next, we will analyze the F-type chain state.

C. Ferromagnetic-type chain state

In this state, the instantaneous spin arrangement is AF along the diagonals and rungs but ferromagnetic along the chains. The key thing to realize is the fact that the Hamiltonian is symmetric with respect to exchanging two spins along the rungs at even sites.[8,13] So, we will get similar spectra if the diagonal terms alternate sign and the terms along the chains have all the same sign (phase π per plaquette). The spectra are the same as for the N-type state except that J_1 and $J_{\times 1}$ are exchanged. Figure 5 illustrates this correspondence.

A similar calculation was done by Dai and Su[29] for the two-leg ladder without diagonal interactions. They chose to alternate the index of the legs along the chain. They argued that this is justifiable because it still preserves the commutation relation when they use the JW transformation and because it gives them the expected results. If you twist their ladder to place the sites that are labeled 1 and 2 so that they each form a leg of the ladder, you will realize that instead of calculating the interaction along the legs of the ladder in the N-type state, they actually consider the interaction along the diagonal for the F-type state.

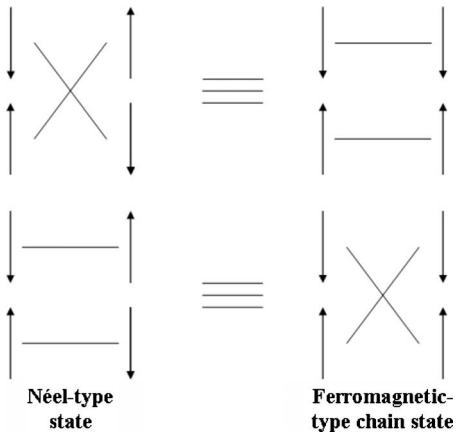

FIG. 5. The coupling along the diagonal (chain) in the N-type state is equivalent to the coupling along the chain (diagonal) in the F-type state.

In their mean-field approach, they end up with better results at $J_\perp/J=1$ (and $J_\times/J=0$) than with the approach of Azzouz *et al.*[21] which we are using here. We are, however, not using their approach because it does not describe properly the limit $J_\perp/J \to 0$. On the contrary, the method we use here describes well this limit. The right description of this limit is crucial for any investigation of the phase diagram.

The bipartite lattice for this state can be seen in Fig. 6. We define two new chains $1'$ and $2'$ which are obtained by relabeling the sites along the diagonals, as indicated in Fig. 6. In this way, the Hamiltonian density we get for the F-type state has the same expression as the one of the N-type state [Eq. (11)] with J_1 replaced by $J_{\times 1}$ and vice versa. Explicitly, the energy eigenvalues are now $\pm E_{F1}$ and $\pm E_{F2}$, with

$$E_{F1}(k) = J_1 \cos k + \sqrt{J_{\times 1}^2 \sin^2 k + \frac{J_{\perp 1}^2}{4}},$$

$$E_{F2}(k) = J_1 \cos k - \sqrt{J_{\times 1}^2 \sin^2 k + \frac{J_{\perp 1}^2}{4}}. \tag{17}$$

The equations for the free energy and the mean-field parameters have the same forms as for the N-type state [Eqs. (14) and (15)], respectively, except that now the partial derivatives of the energies with respect to Q, P, and P' are

$$\frac{\partial E_{Fp}}{\partial Q} = 2J \cos k,$$

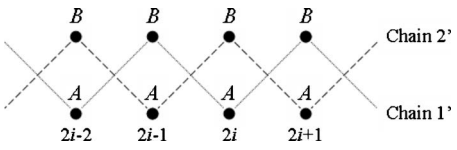

FIG. 6. The lattice is drawn in the case of the F-type state.

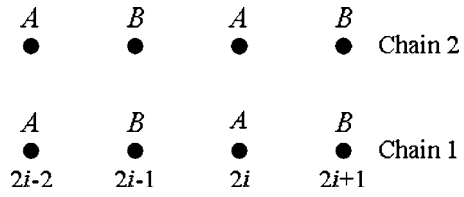

FIG. 7. The bipartite character of the lattice in the case of the *R*-type state is shown.

$$\frac{\partial E_{Fp}}{\partial P} = \frac{(-1)^{p+1} J_{\perp} J_{\perp 1}}{2\sqrt{J_{\times 1}^2 \sin^2 k + \frac{J_{\perp 1}^2}{4}}},$$

$$\frac{\partial E_{Fp}}{\partial P'} = \frac{(-1)^{p+1} 2 J_{\times} J_{\times 1} \sin^2 k}{\sqrt{J_{\times 1}^2 \sin^2 k + \frac{J_{\perp 1}^2}{4}}} \quad \text{with } p = 1,2. \tag{18}$$

D. Ferromagnetic-type rung state

This state is realized when the spin arrangement at any time is such that the spins along the diagonals are antiparallel and the spins along the rungs are parallel. The bipartite lattice for this state is displayed in Fig. 7. In this state, both the diagonal and the chain terms link *A* and *B* fermions and vice versa, i.e., they are AF. Based on our previous arguments in Sec. II B, a phase of π per plaquette can be used, with the mean-field phase this time alternating between 0 and π along the chains like in the *N*-type state.

A 1D Fourier transform is performed along the chains while keeping the chain labels in real space. The mean-field Hamiltonian has the same expression as Eq. (9) with the Nambu spinor now defined by

$$\Psi^{\dagger} = (c_{1k}^{A\dagger}\ c_{2k}^{A\dagger}\ c_{1k}^{B\dagger}\ c_{2k}^{B\dagger}), \tag{19}$$

and the Hamiltonian density given by

$$\mathcal{H} = \begin{pmatrix} 0 & \frac{J_{\perp 1}}{2} & iJ_1 \sin k & J_{\times 1} \cos k \\ \frac{J_{\perp 1}}{2} & 0 & J_{\times 1} \cos k & iJ_1 \sin k \\ -iJ_1 \sin k & J_{\times 1} \cos k & 0 & \frac{J_{\perp 1}}{2} \\ J_{\times 1} \cos k & -iJ_1 \sin k & \frac{J_{\perp 1}}{2} & 0 \end{pmatrix}. \tag{20}$$

Diagonalizing this matrix yields the energy eigenvalues $\pm E_{R1}$ and $\pm E_{R2}$ with

$$E_{R1}(k) = \frac{J_{\perp 1}}{2} + \sqrt{J_1^2 \sin^2 k + J_{\times 1}^2 \cos^2 k},$$

$$E_{R2}(k) = \frac{J_{\perp 1}}{2} - \sqrt{J_1^2 \sin^2 k + J_{\times 1}^2 \cos^2 k}. \tag{21}$$

Again, the equations for the free energy and the mean-field parameters have the same form as for the *N*-type state, with the partial derivatives of the energies with respect to Q, P, and P' replaced by

$$\frac{\partial E_{Rp}}{\partial Q} = \frac{(-1)^{p+1} 2 J J_1 \sin^2 k}{\sqrt{J_1^2 \sin^2 k + J_{\times 1}^2 \cos^2 k}},$$

$$\frac{\partial E_{Rp}}{\partial P} = J_{\perp},$$

$$\frac{\partial E_{Rp}}{\partial P'} = \frac{(-1)^{p+1} 2 J_{\times} J_{\times 1} \cos^2 k}{\sqrt{J_1^2 \sin^2 k + J_{\times 1}^2 \cos^2 k}} \quad \text{with } p = 1,2. \tag{22}$$

Now that we have derived the mean-field equations for all three states, we solve them in order to get the zero-temperature and temperature-dependent phase diagrams. These equations are solved numerically, except in the high-temperature limit where they are solved both analytically and numerically. Our results will be compared with existing exact numerical data.

III. RESULTS

A. Zero-temperature phase diagram

The free (ground-state) energies of all three states are calculated as functions of coupling constants and compared. From thermodynamic considerations, the state with the lowest free energy is the stable one, and whenever free energies cross a phase transition takes place. Since only the ratios of the couplings are important, we define $\alpha_1 = J_{\perp}/J$ and $\alpha_2 = J_{\times}/J$. The calculation was carried out for different sets of values of α_1 and α_2, with J being the unit of energy. We found that at some values of these couplings, free energies cross, which means that a phase transition occurs. You can refer to Fig. 8 for a couple of examples. In this way, we have obtained the phase diagram at zero temperature. The phase transitions found here using BMFT are first-order ones for all values of α_2. This agrees relatively well with most of the work done thus far by numerical[8,9] and analytical methods.[15] For small α_2, most numerical methods lacked the required accuracy to determine the order of the transition, but the DMRG calculation by Wang[13] found that for $\alpha_2 < 0.287$ the transition is of second-order character, and for all larger values it is first order. Because these transitions take place at zero T as a consequence of varying the diagonal interaction, they can be labeled as quantum phase transitions.[1] Experimentally for a real material, one can vary the pressure and hope that the diagonal (or any other) coupling changes enough so that the critical region is reached. The (α_1, α_2)-phase diagram we calculated is compared to the Lanczos-technique data of Ref. 8 in Fig. 9. The agreement between the Lanczos method data and our results is very good, a fact that indicates that the present mean-field treatment is acceptable. The line at $\alpha_2 = 1$ is exact and its place-

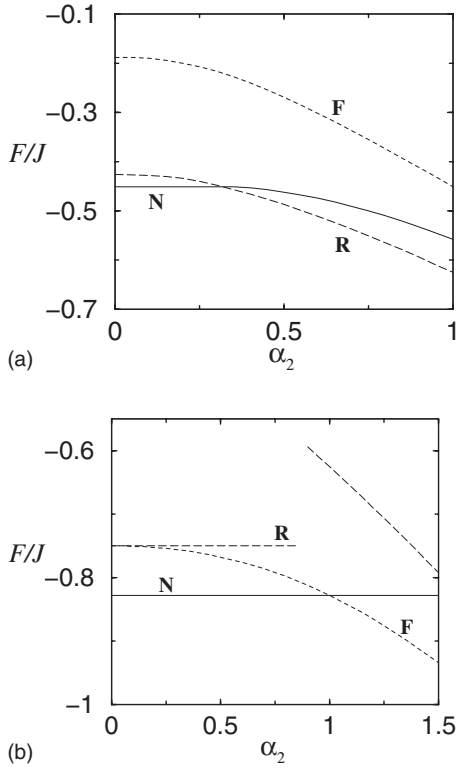

FIG. 8. The zero-T free (ground-state) energies as calculated by BMFT for the N-type state (N), R-type state (R), and the F-type state (F) are plotted versus $\alpha_2=J_\times/J$. (a) $\alpha_1=J_\perp/J=0.5$; there is a transition from the N-type state to the R-type state. (b) $\alpha_1=2$; there is a transition from the N-type state to the F-type state. There is a discontinuity in the free energy of the R-type state due to a sudden change in the bond parameters. This is of no interest because the only stable state is the one with the lowest free energy, and the transition is determined by the crossing of the lower free energies.

ment is a consequence of the Hamiltonian symmetry with respect to exchanging J and $J_\times$, which BMFT fully satisfies.

B. Mean-field parameters

The mean-field bond parameters Q, P, and P' are not order parameters in the conventional way because they are not related in any way to any sort of long-range order. In BMFT, they are a measure of the AF fluctuations in the system. Each of these parameters can be interpreted as indicating the presence of a strong spin bond in the spatial direction in which this parameter is found to be significant. The spin bond consists of a renormalized spin singlet formed on adjacent lattice sites. It is therefore important to know the coupling dependence of these parameters. We found that it is the combination of how these parameters and free energies depend on coupling constants that determines the phase boundaries between the three possible states; N-type, R-type, and F-type. The zero-T mean-field parameters are plotted in Fig. 10 as functions of α_2 and α_1. From the analysis of free energy, we determine the initial and final states as well as the transition points. In each state, the parameter that is zero corresponds to the direction with ferromagnetic arrangement.

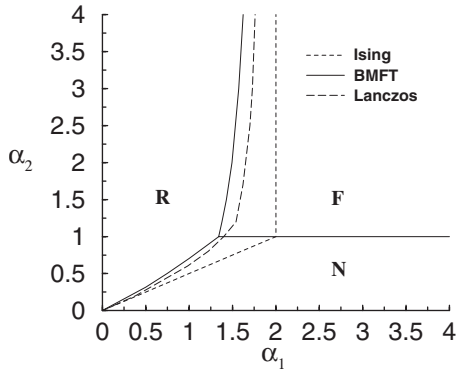

FIG. 9. The (α_1,α_2)-phase diagram we calculate is shown. It is compared to the Lanczos method (Ref. 8) and Ising expansion (Ref. 8) results. The boundaries are between the N-type state (N), R-type state (R), and the F-type state (F). For comparison, the phase boundaries (dotted lines) in the Ising limit are also shown.

For example, in Fig. 10(a) for small α_2, we are in the N-type state with $P'=0$ and other parameters (Q and P) hardly changing as α_2 increases. At $\alpha_2=0.7$, there is a transition to the R-type state, which is accompanied by a sharp change where P vanishes and P' increases sharply.

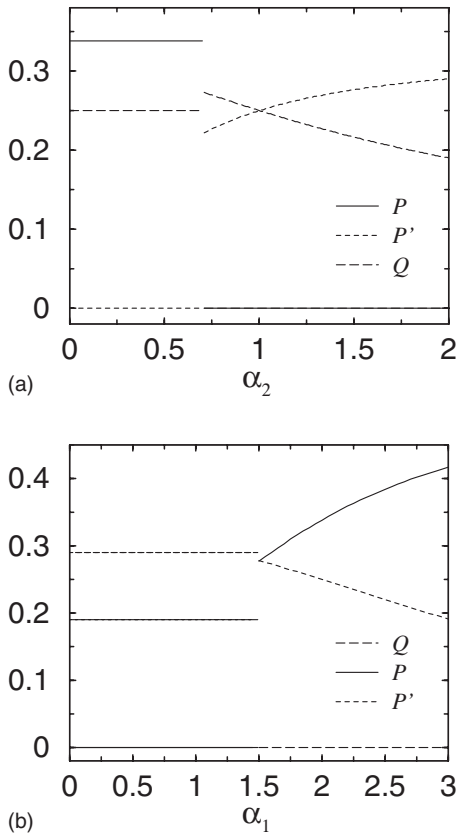

FIG. 10. (a) The mean-field parameters are displayed as functions of α_2 for $\alpha_1=1$. There is a transition from the N-type state to the R-type state at $\alpha_2=0.7$. (b) The mean-field parameters are displayed as functions of α_1 for $\alpha_2=2$. There is a transition from the R-type state to the F-type state at $\alpha_1=1.5$.

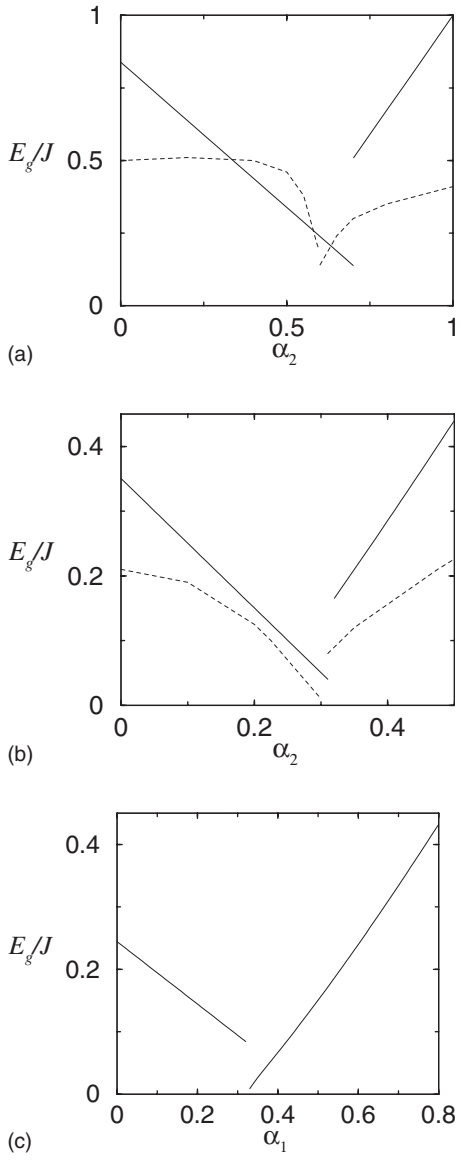

FIG. 11. (a) The energy gap calculated for $\alpha_1=1$ as a function of α_2 is displayed. The solid line is the data calculated using BMFT and the dotted one is the DMRG data from Ref. 13. (b) The energy gap plotted for $\alpha_1=0.5$ as a function of α_2. The solid line is the data calculated using BMFT and the dotted one is the DMRG data from Ref. 14. (c) The energy gap is plotted as a function of α_1 for $\alpha_2=0.2$.

C. Energy gap and spectra

Another quantity of significant importance is the energy gap, which characterizes all three states. As a consequence, all spin correlations span regions of size of the order of the reciprocal of the gap. We calculated the gap as a function of α_2 for $\alpha_1=1$ and reported it in Fig. 11. Our result is compared to the exact DMRG ones[13,14] in the same figure. One can note that the gap we calculate is not in good quantitative agreement, but as far as trends are concerned good qualitative agreement is found. Our gap behaves linearly in all the mean-field calculations, whereas in the DMRG it is nearly horizontal for small and large values of α_2. The most important feature that both BMFT and DMRG results share is that the gap shows a minimum at the critical value of α_2. In the DMRG results,[13] the transition was interpreted to be second order for $\alpha_2<0.287$ because the gap vanishes (within uncertainty) at the transition. In BMFT, the transition is not gapless but the gap becomes very small. For $\alpha_2=0.2$, the minimum gap value from DMRG[13] is $0.004J\pm0.004J$, and in BMFT it is $0.009J$. One should stress, however, that it is the crossing of the free (or ground-state) energies that determines the transitions in BMFT not the vanishing of the energy gap.

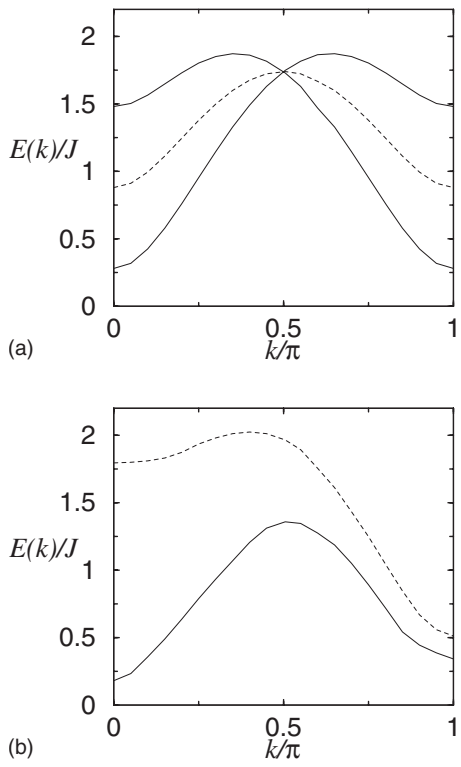

FIG. 12. (a) The energy spectra calculated within BMFT (dotted lines) are compared to those from the dimer-expansion method of Ref. 8 (solid lines). In (a) $\alpha_1=1$, $\alpha_2=0$, and in (b) $\alpha_1=1$, $\alpha_2=0.6$.

The energy spectra for $\alpha_1=1$ and $\alpha_2=0$ and for $\alpha_2=0.6$ both in the N-type state are shown in Fig. 12. For $\alpha_1=1$ and zero diagonal coupling, the exact spectrum calculated numerically starts off asymmetric with a minimum at $k=\pi$.[8,30] As frustration increases, the local minimum at 0 decreases rapidly but the absolute minimum at π decreases only slowly. So, the energy gap decreases slowly while the minimum is at π but starts to decrease rapidly once the absolute minimum shifts to $k=0$.

Within the BMFT, the shape of the spectrum for $\alpha_1=1$ and $\alpha_2=0$ is different from the exact one. However, as discussed in Ref. 24, the important feature shared by both results is the presence of an energy gap. Also, BMFT rightfully describes the physics of the two-leg ladder in this limit, namely, that the ground state consists of the formation of renormalized spin singlets on the rungs. The difference in the curves for the energy gap (Fig. 11) is due to the complex behavior of the spectra shape as the couplings are varied. Near the boundary line between R- and N-type states, for

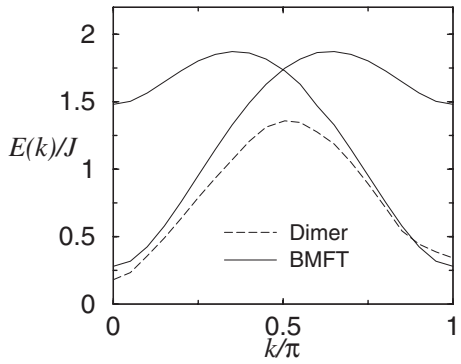

FIG. 13. Comparison of spectra for $\alpha_2=0.6$. The dashed curve is the result of the dimer expansion in Ref. 8.

$\alpha_1=1$ and $\alpha_2=0.6$, the BMFT spectra yield a low-lying excitation spectrum that overall behaves like the dimer-expansion data of Ref. 8; see Fig. 13.

D. Nonzero-temperature phase diagram

Unlike exact diagonalization methods, the present analytical approach can be readily used to analyze the effects of temperature on the system. We repeated the same approach as in Sec. III A by comparing the free energies of the three phases, this time, at different temperatures for various sets of coupling values. We deduced the temperature dependence of the phase boundaries in the phase diagram. The result of such a calculation is reported in Fig. 14. We found that as the temperature increases, the *R*-type state decreases in size. The sizes of the *N*-type and *F*-type phases increase with temperature.

In the *R*-type state at zero temperature, the spins on the rungs arrange themselves ferromagnetically; notice that on any rung, the pair of spins fluctuates together between the up and down spin orientations, while the two pairs of spins on the adjacent rungs fluctuate in the opposite direction. So, the system is neither ordered ferromagnetically nor antiferromagnetically. As mentioned earlier, the parameter P is a measure of the AF correlations along the rung direction. Because of the ferromagnetic orientation, their AF correlations are zero, leading to $P=0$. This parameter becomes nonzero as the temperature increases, as seen in Fig. 15, because thermal fluctuations allow the rungs to adopt sometimes the

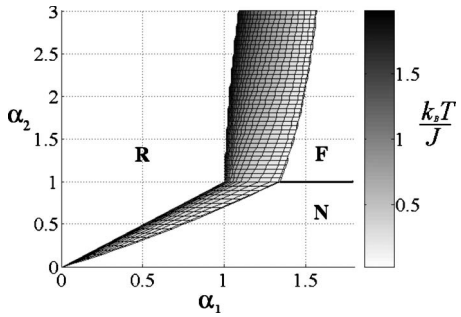

FIG. 14. Surface plot of the phase diagram showing the temperature dependence.

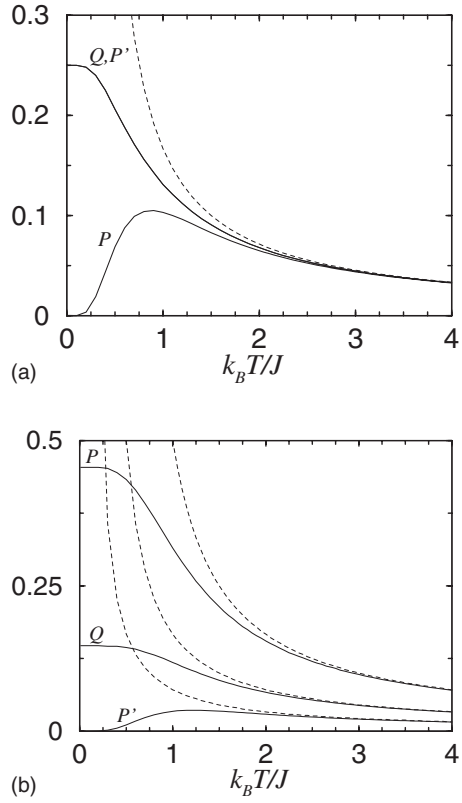

FIG. 15. The mean-field parameters are plotted versus temperature (solid lines). The dotted lines are from the high-temperature limit equations [Eq. (23)]. (a) $\alpha_2=\alpha_1=1$ in the *R*-type state. (b) $\alpha_2=0.5$ and $\alpha_1=2$ in the *N*-type state.

AF arrangement. Note that eventually, the AF correlations diminish in the very high-temperature limit, a fact that is indicated by P decreasing as $1/T$ after reaching a maximum. In the Ising limit, the phase boundary between the *R*-type and *N*-type phases is $\alpha_1=2\alpha_2$, and the boundary between the *R*-type and *F*-type phases is $\alpha_1=2$. Quantum fluctuations cause these phase boundaries to move toward the *R*-type state. Including thermal fluctuations seems to have the same effect. It is found that as the temperature increases, the phase boundaries move toward $\alpha_1=\alpha_2$ and $\alpha_1=1$, respectively. As the temperature rises, P approaches but never becomes larger than P' and Q for $\alpha_1=\alpha_2=1$, Fig. 15.

E. High-temperature regime

In the limit $k_BT \gg J$, $J_\perp$, and $J_\times$, the mean-field equations can be solved analytically. The Fermi-Dirac factors (tanh functions) can be expanded to first order in βE_p in the mean-field equations.[24] The approximation is subbed into Eqs. (15) with $\Sigma_k \to \int \frac{dk}{2\pi}$, and the following set of equations are obtained:

$$Q \approx \frac{J}{8k_BT\left(1-\frac{J}{4k_BT}\right)}, \quad k_BT \gg J,$$

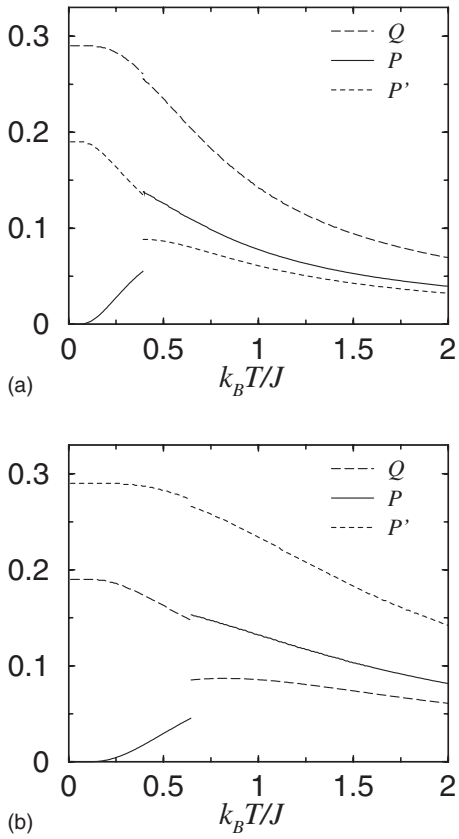

FIG. 16. The parameters are plotted versus temperature for two coupling sets. (a) $\alpha_2=0.5$ and $\alpha_1=0.6$. The phase transition happens at $k_BT/J=0.39$ from the R-type to the N-type state. (b) $\alpha_2=2$ and $\alpha_1=1.25$. The phase transition happens at $k_BT/J=0.64$ from the R-type to the F-type state.

$$P \approx \frac{J_\perp}{8k_BT\left(1-\frac{J_\perp}{4k_BT}\right)}, \quad k_BT \gg J_\perp,$$

$$P' \approx \frac{J_\times}{8k_BT\left(1-\frac{J_\times}{4k_BT}\right)}, \quad k_BT \gg J_\times. \tag{23}$$

We find that these equations are independent of the state in which they are calculated; i.e., whether we use the set of equations for the N-type, R-type, or F-type state, we always get the same result [Eq. (23)] in the high-T regime. In this regime, the parameters decrease following a Curie-Weiss T^{-1} law but never vanish, excluding in this way the occurrence of any finite-temperature phase transition from a state with finite spin bond order to a high-T state with zero spin bond order. Note that Eqs. (23) fit very well the numerically calculated parameters, as seen in Fig. 15. It is interesting to note that all the parameters have the same form and show the same dependence on the ratio of the coupling constant, in the direction in which the parameter is calculated, and temperature. Note that the smallest parameter corresponds to the direction in which the spins are ferromagnetically arranged, e.g., P is the smallest parameter in the R-type state. At high temperature, it is easy to see from Eq. (23) that the parameter corresponding to the smallest coupling value will be smallest. So, in the high-temperature limit, the largest coupling value determines the state of the system. This is why the boundaries in the phase diagram shift to $\alpha_1=\alpha_2$ and $\alpha_1=1$.

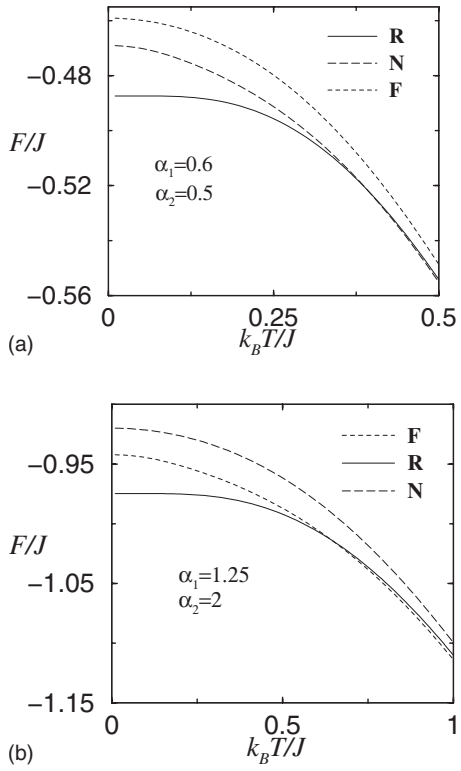

FIG. 17. The free energies are plotted as functions of temperature. The phase transitions happen where the free energies cross. (a) $\alpha_2=0.5$ and $\alpha_1=0.6$. The phase transition happens at $k_BT/J=0.39$ from the R-type to the N-type state. (b) $\alpha_2=2$ and $\alpha_1=1.25$. The phase transition happens at $k_BT/J=0.64$ from the R-type to the F-type state.

IV. CRITICALITY AT NONZERO TEMPERATURE

For sets of coupling values (α_1,α_2) within the shaded region of Fig. 14, the thermal fluctuations can cause a first-order phase transition from the R-type state to the F-type state or N-type state. There are no thermally induced transitions between the F-type and N-type states because the boundary between the N- and F-type states is not temperature dependent due to the symmetry of the Hamiltonian with respect to exchanging J and $J_\times$ terms. Note that thermally induced transitions are not from a disordered phase to an ordered one or vice versa. The mean-field bond parameters are displayed in Fig. 16 as functions of temperature for two sets of couplings α_1 and α_2 such that Fig. 16(a) shows a transition from the R-type to the N-type state and Fig. 16(b) shows a transition from the R-type to the F-type state. The corresponding free energies are shown in Fig. 17, entropies in Fig. 18, and specific heats in Fig. 19 for the same sets of couplings.

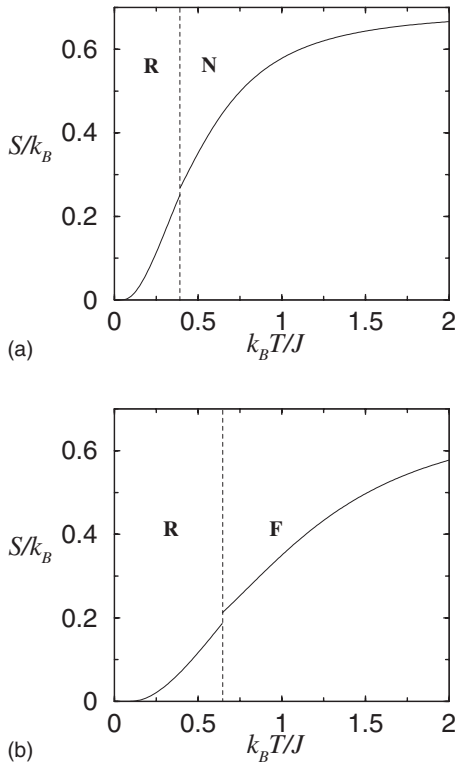

FIG. 18. The entropy is plotted versus temperature. The entropy is discontinuous at the transition points. The dashed lines indicate the transition between the different phases. (a) $\alpha_2=0.5$ and $\alpha_1=0.6$. The phase transition happens at $k_BT/J=0.39$ from the R-type to the N-type state. (b) $\alpha_2=2$ and $\alpha_1=1.25$. The phase transition happens at $k_BT/J=0.64$ from the R-type to the F-type state.

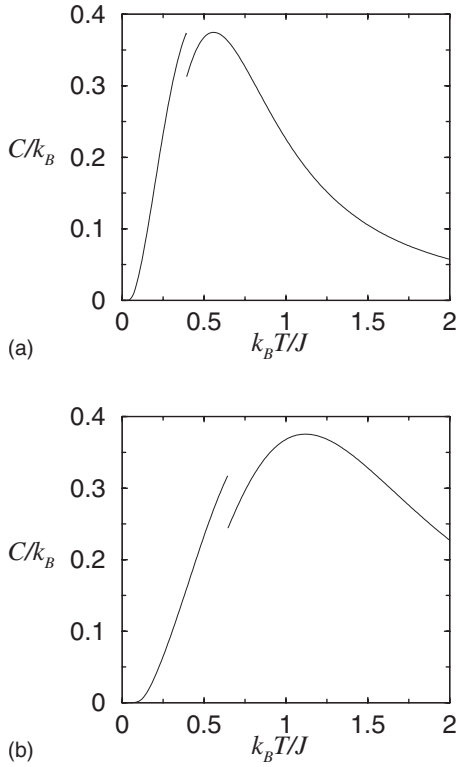

FIG. 19. The specific heat is calculated by $C=T\frac{\partial S}{\partial T}$. The infinite peaks at the transitions, which are a consequence of the discontinuity in $S(T)$, are not displayed for clarity. (a) $\alpha_2=0.5$ and $\alpha_1=0.6$. The phase transition happens at $k_BT/J=0.39$ from the R-type to the N-type state. (b) $\alpha_2=2$ and $\alpha_1=1.25$. The phase transition happens at $k_BT/J=0.64$ from the R-type to the F-type state.

The entropy is calculated using

$$S=-\frac{k_B}{2N}\sum_k\sum_{p=1}^{4}(n_F[E_p(k)]\ln\{n_F[E_p(k)]\} + \{1-n_F[E_p(k)]\}\ln\{1-n_F[E_p(k)]\}), \quad (24)$$

which is derived from $S=-\frac{\partial F}{\partial T}$. In Eq. (24), $E_p(k)$ refers to the energy spectra of the state where S is calculated. The specific heat is calculated using $C=T\frac{\partial S}{\partial T}$. The entropy shows a discontinuity at T_C, implying that the transition is first order in character. At very high temperature, entropy saturates as expected to a value of $k_B\ln 2$. In Fig. 18(a) for $\alpha_2=0.5$ and $\alpha_1=0.6$, the phase transition happens at $k_BT/J=0.39$ from the R-type to the N-type state when T increases. In Fig. 18(b) with $\alpha_2=2$ and $\alpha_1=1.25$, the phase transition happens at $k_BT/J=0.64$ from the R-type to the F-type state. In these figures, the dashed lines simply indicate the transitions between the different phases corresponding to the set of couplings used. We found that in the limit α_1 and $\alpha_2\to 0$, the jump in entropy goes to zero. For small coupling values, this jump could be smaller than the experimental precision (if a real material existed) so that it would become difficult to assert that the transition is a first-order one. For example, for $\alpha_2=0.2$ and $\alpha_1=0.24$, the jump in entropy is about $0.002k_B$ only. Note that because all three states are gapped, both entropy and specific heat show an activated behavior in the vicinity of zero temperature.

All the phases of the system are disordered, i.e., none of them is characterized by the long-range magnetic order of any kind. The proposed thermally induced criticality can be seen as a remnance of the zero-T (quantum) criticality because of the temperature dependence of the phase boundaries. As mentioned earlier in the Introduction, the mean-field parameters Q, P, and P' do not represent any kind of long-range order. The zero-temperature phase transitions we analyzed in Sec. III A all occur between disordered phases that differ only by the way the spins arrange themselves on very short distances (refer to Fig. 2). Therefore, we believe that the finite-T transitions we find here for the present practically one-dimensional system are not an artifact of the mean-field character of BMFT. These phase transitions are due to frustration, i.e., they disappear once frustration is brought to zero. They are also a consequence of the fact that the zero-T quantum phase transition boundary depends on temperature. Because zero temperature cannot be reached in practice, a quantum phase transition cannot, in fact, be observed directly. For the present system, the signature for such a transition would be the observation of the finite-T transitions (if an experimental system existed).

V. DISCUSSION

While the quantum criticality we find in this system has been already found elsewhere using exact numerical methods, the criticality at finite temperature we report on here remains to be confirmed by other theoretical methods. Experimentally, if ever a frustrated two-leg ladder where the strength of frustration is as important as the coupling along the rungs and chains existed, then thermodynamical measurements would either confirm or refute our claims. Perhaps, the application of a high pressure on a two-leg ladder material could increase the diagonal interaction and allow the search for this thermally induced criticality. In the absence of diagonal interaction (frustration), the AF Heisenberg two-leg ladder shows neither quantum nor classical criticality. Interestingly, it is the frustration that is responsible for both criticalities. A strong argument in favor of the existence of the finite-T criticality is the existence of the zero-T one itself because in both cases each phase boundary separates two of the same three disordered phases. Denying the finite-T criticality would amount to denying the zero-T one according to the present theory.

VI. CONCLUSION

In this work, we studied quantum as well as classical criticality in the two-leg ladder with exchange interactions along the chains, rungs, and diagonals using the Jordan-Wigner transformation and the bond-mean-field theory. The zero-temperature phase diagram of this system is calculated. We found it to exhibit three quantum phases, characterized all by an energy gap and the absence of magnetic order. These states are labeled Néel-type (N-type), rung-type (R-type or Haldane-type), and ferromagnetic-type chain (F-type) states. This result agrees well with existing numerical data. The transitions from one phase to any of the two others are all first order. Because they occur at zero temperature, they enter under the category of quantum phase transitions. When temperature increases for some sets of coupling values, the system undergoes a phase transition from the R-type state to the N- or F-type state at a finite temperature. The finite temperature phase diagram is calculated as well. In it, the size of the R-type state becomes smaller while the F-type state and the N-type state increase in size with increasing temperature. The good agreement between our results and existing exact results for the zero-T phase diagram suggests that the present mean-field treatment is acceptable. The various phase transitions found in this work occur between magnetically disordered states. It is solely the frustration, the spin bond parameters, and the nature of short-range magnetic correlations that determine the nature of all three phases that characterize the frustrated antiferromagnetic Heisenberg two-leg ladder. In the present mean-field-type approach, all phase transitions are first order in character. While at zero temperature existing exact numerical data seem to indicate that this is the case, at finite temperature the degree of the transitions remains to be confirmed.

ACKNOWLEDGMENT

We wish to acknowledge the financial support of the Natural Science and Engineering Research Council of Canada (NSERC).

*mazzouz@laurentian.ca

[1] S. Sachdev, in *Quantum Phase Transitions* (Cambridge University Press, New York, 1999).
[2] For a review, see E. Dagotto and T. M. Rice, Science **271**, 618 (1996).
[3] M. Azuma, Z. Hiroi, M. Takano, K. Ishida, and Y. Kitaoka, Phys. Rev. Lett. **73**, 3463 (1994).
[4] C. A. Hayward, D. Poilblanc, and L. P. Lévy, Phys. Rev. B **54**, R12649 (1996).
[5] G. Chaboussant, P. A. Crowell, L. P. Lévy, O. Piovesana, A. Madouri, and D. Mailly, Phys. Rev. B **55**, 3046 (1997).
[6] T. Imai, K. R. Thurber, K. M. Shen, A. W. Hunt, and F. C. Chou, Phys. Rev. Lett. **81**, 220 (1998).
[7] M. Matsuda, K. Katsumata, R. S. Eccleston, S. Brehmer, and H.-J. Mikeska, J. Appl. Phys. **87**, 6271 (2000).
[8] Zheng Weihong, V. Kotov, and J. Oitmaa, Phys. Rev. B **57**, 11439 (1998).
[9] T. Sakai and N. Okazaki, J. Appl. Phys. **87**, 5893 (2000).
[10] H.-H. Hung, C.-D. Gong, Y.-C. Chen, and M.-F. Yang, Phys. Rev. B **73**, 224433 (2006).
[11] S. R. White, Phys. Rev. B **53**, 52 (1996).
[12] T. Hakobyan, J. H. Hetherington, and M. Roger, Phys. Rev. B **63**, 144433 (2001).
[13] X. Q. Wang, Mod. Phys. Lett. B **14**, 327 (2000).
[14] N. Zhu, X. Wang, and C. Chen, Phys. Rev. B **63**, 012401 (2000).
[15] Y. Xian, Phys. Rev. B **52**, 12485 (1995).
[16] D. Allen, F. H. L. Essler, and A. A. Nersesyan, Phys. Rev. B **61**, 8871 (2000).
[17] T. Hakobyan, Phys. Rev. B **75**, 214421 (2007).
[18] O. A. Starykh and L. Balents, Phys. Rev. Lett. **93**, 127202 (2004).
[19] C.-M. Nedelcu, A. K. Kolezhuk, and H.-J. Mikeska, J. Phys.: Condens. Matter **12**, 959 (2000).
[20] D. C. Cabra, A. Dobry, and G. L. Rossini, Phys. Rev. B **63**, 144408 (2001).
[21] M. Azzouz, L. Chen, and S. Moukouri, Phys. Rev. B **50**, 6233 (1994).
[22] B. Bock and M. Azzouz, Phys. Rev. B **64**, 054410 (2001).
[23] M. Azzouz, Phys. Rev. B **48**, 6136 (1993).
[24] M. Azzouz, Phys. Rev. B **74**, 174422 (2006).
[25] E. H. Kim, G. Fàth, J. Sólyom, and D. J. Scalapino, Phys. Rev. B **62**, 14965 (2000).
[26] N. D. Mermin and H. Wagner, Phys. Rev. Lett. **17**, 1133 (1966).
[27] I. Affleck and J. B. Marston, Phys. Rev. B **37**, 3774 (1988).
[28] J. des Cloiseaux and J. J. Pearson, Phys. Rev. **128**, 2131 (1962).
[29] X. Dai and Z.-b. Su, Phys. Rev. B **57**, 964 (1998).
[30] T. Barnes, E. Dagotto, J. Riera, and E. S. Swanson, Phys. Rev. B **47**, 3196 (1993).